Journal of Functional Materials and Applied Engineering

Review Paper

Application of Black Titanium Dioxide and Its Composite Materials in Photocatalytic Degradation of Water Pollutants

Arthur Conan Doyle [1], **Hercule Poirot** [2,*]
[1] University of Klagenfurt, Klagenfurt, Austria
[2] School of Life Sciences, Busan University of Foreign Studies, Busan, South Korea
*Corresponding author: ACDoyle@gmail.com; Poirotvs11@gmail.com

Abstract. Photocatalysis, prized for its effectiveness, environmental soundness, and affordability, is finding promise across an ever-widening range of uses. Titanium dioxide (TiO_2) remains the benchmark photocatalyst, yet its inherently broad bandgap restricts activation to ultraviolet wavelengths, while rapid electron–hole recombination additionally saps its efficiency. Black titanium dioxide (TiO_{2-x}), formed by embedding surface defects — oxygen vacancies above all — overcomes these limitations: the shrunken bandgap together with the proliferation of active sites strengthens its response and quantum yield throughout the visible and near-infrared regions, elevating overall catalytic performance. Consequently, how TiO_{2-x} is synthesized, modified, and incorporated into composites has become a subject of intense investigation. Herein, we delineate the principal defect architectures of TiO_{2-x} and the analytical methods suited to probing them, recapitulate its major fabrication routes, and review available modification strategies. Particular attention is devoted to the behavior of TiO_{2-x} and its hybrids in degrading aqueous pollutants, with the relevant decomposition mechanisms dissected and consolidated. We close by appraising the obstacles and opportunities that will shape the deployment of TiO_{2-x}-based materials in future water-remediation efforts.

Keywords: *black titanium dioxide; modified materials; photocatalysis; water pollutants; degradation mechanisms*

Received on 02 July 2024, Accepted on 05 Nov 2024, Published on 15 Dec 2024

Copyright © 2024 Arthur Conan Doyle and Hercule Poirot licensed to JFMAE. This is an open access article distributed under the terms of the CC BY-NC-SA 4.0, which permits copying, redistributing, remixing, transformation, and building upon the material in any medium so long as the original work is properly cited.

1 Introduction

Photocatalysis is a green approach in which light energy drives redox processes at the surface of a material[1]. Since it operates without additional chemical reagents or external heating, it carries vast potential for use in many fields[2]. Among semiconductor photocatalysts, titanium dioxide (TiO_2) has been the most intensively explored, valued for its affordability, lack of toxicity, and ease of preparation[3-4]. Ordinary white TiO_2 is constrained by its 3.0–3.2 eV bandgap, which limits activation to ultraviolet light and leaves most of the solar spectrum untapped; worse still, defects buried in the bulk or residing at metastable surface sites serve as recombination hubs where electrons and holes annihilate one another, draining the pool of usable photogenerated carriers[5-7]. The turning point arrived in 2011 with the work of CHEN et al.[8], who exposed white TiO_2 to hydrogen under elevated temperature and pressure and thereby created black, oxygen-deficient titanium dioxide, TiO_{2-x} ($0<x<2$). Endowed with a bandgap compressed to just 1.54 eV alongside plentiful oxygen vacancies and Ti^{3+} ions, this variant absorbs light far more effectively and displays superior photocatalytic activity. Hydrogenation simultaneously wraps the particles in a disordered core–shell skin roughly 1 nm thick, which ties off unsaturated surface bonds and lends the material greater robustness. It is precisely the combined presence of surface disorder, vacancies, and Ti^{3+} that grants TiO_{2-x} seamless photon capture stretching from the ultraviolet (UV) all the way into the near-infrared (NIR). Under sustained operation, however, such surface defects can gradually poison active sites, eroding recyclability, and the very bandgap narrowing that boosts light uptake may likewise impede efficient electron–hole separation[9]. Realizing the full practical value of TiO_{2-x} thus requires additional engineering interventions — metal deposition, non-metal doping, and heterojunction assembly among them — to lift both quantum efficiency and cycling endurance. The compelling results achieved by TiO_{2-x} and its hybrid systems in decomposing aqueous pollutants have accordingly spurred a surge of research attention

in recent years [10-11].

Against this background, and with reference to the relevant characterization methods, the present review organizes the principal defect structures of TiO_{2-x} and provides an overview of its preparation routes and modification strategies. It puts special emphasis on analyzing practical scenarios where TiO_{2-x} and derived composites photocatalytically degrade water-borne pollutants, conducts profound analysis and generalization of corresponding degradation mechanisms, and identifies challenges and prospects confronting TiO_{2-x} within this research domain.

2 Defect Structures of TiO_{2-x} and Their Characterization Approaches

2.1 Surface Disordered Structure

Reductive processing, exemplified by hydrogenation, reorganizes the crystal surface of TiO_{2-x} and coats it with a disordered sheath, giving rise to a core–shell architecture in which a crystalline interior is wrapped by an amorphous exterior. This disordered shell is populated with numerous defect species — oxygen vacancies, Ti^{3+} ions, and Ti–H as well as O–H bonds — which collectively facilitate charge-carrier separation, widen the spectral range of absorption, and intensify light harvesting[12]. Experimental verification of these disordered surface layers relies on techniques such as high-resolution transmission electron microscopy (HRTEM), Raman spectroscopy, and X-ray diffraction (XRD), with representative results displayed in Figure 1.

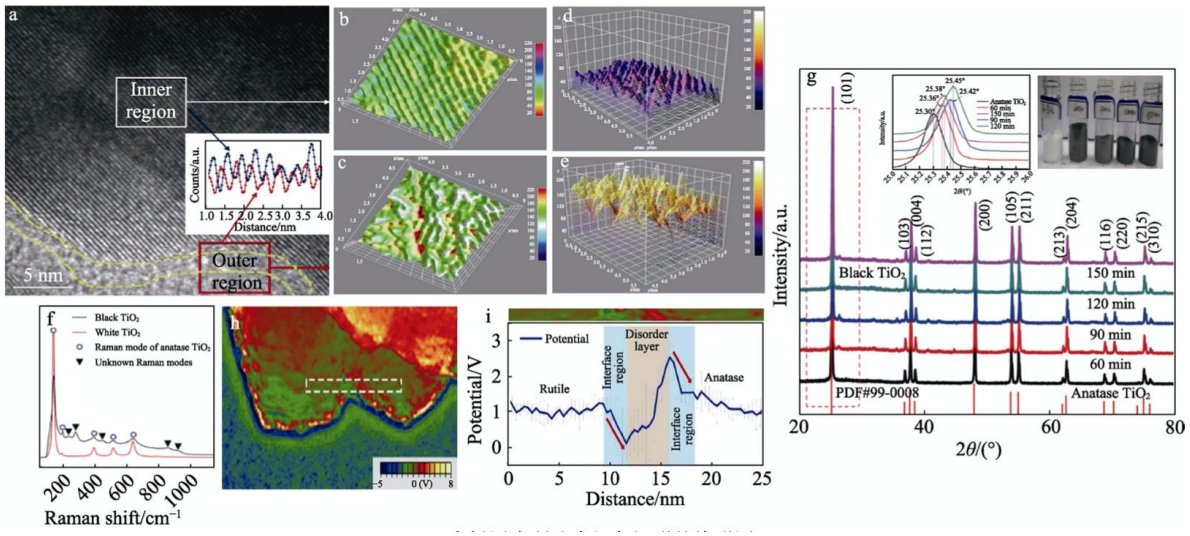

Figure 1 HRTEM image (a) and its 3D schematic diagram (b~e), Raman spectrum (f), electric potential diagram (h~i), XRD patterns (g) of TiO2–x[13-18]

HRTEM functions by focusing electron beams transmitted through TiO_{2-x} with electromagnetic lenses for imaging observations. It validates the formation of outer disordered shells in core-shell architectures through detecting lattice distortion and shifts in interplanar spacing[13]. Figure 1a highlights, by means of a yellow dashed contour around the crystalline core, an outer disordered sheath about 1 nm thick enveloping the particle interior. Three-dimensional reconstructions of the region inside the white box (Figure 1b, c) reveal an inner core composed of regularly ordered, atomically flat facets, whereas the corresponding views of the red-boxed region (Figure 1d, e) show a shell whose long-range atomic order is disrupted, verifying that the outermost layer is disordered and defect-rich[14]. Structural information is also accessible through Raman scattering: relative to untreated TiO_2, the TiO_{2-x} spectrum in Figure 1f contains additional, otherwise unassigned bands at 238, 280, 447, 854, and 916 cm^{-1}[15], all traceable to the disordered surface architecture[16]. Complementary evidence comes from XRD, which probes crystallinity via angle-dependent diffraction intensities. As Figure 1g illustrates, the disordered shell partially degrades crystalline perfection and displaces diffraction peaks — although TiO_{2-x} retains appreciable crystallinity overall, extended sintering pushes the (101) reflection toward higher angles, a signature of lattice strain imposed on the reduced material by surface disorder[17]. This picture is further corroborated by potential-

DOI:

distribution mapping (Figure 1h, i), where abrupt potential drops occur precisely at the two boundaries dividing the crystalline and disordered domains[18]. Clarifying the manner in which individual defect populations within the disordered shell dictate the behavior of TiO_{2-x} therefore calls for a dedicated, species-by-species invtigation.

2.2 Oxygen Vacancies and Ti^{3+}

Among the defects hosted in the disordered shell of TiO_{2-x}, oxygen vacancies and Ti^{3+} ions stand out as the two most consequential. Vacancies form when oxygen atoms abandon their lattice positions and accumulate preferentially at the surface, where they help pull photogenerated electrons and holes apart, raising catalytic efficiency in the process[19]. Density functional theory (DFT) studies covering TiO_{2-x} stoichiometries between \(1.75<x<2.00\) show titanium coordination numbers varying from 5 to 7, with the average oxygen coordination climbing in step with the reduction degree — a trend that corroborates vacancy formation at the surface[20]. Ti^{3+} species, arising either from Ti^{4+} reduction or oxidation of lower-valence titanium, embed mid-gap states into the electronic structure; the attendant bandgap contraction pushes light absorption into the visible range and markedly improves solar-energy harvesting[21-23]. Techniques suited to detecting both defect families include ultraviolet–visible diffuse-reflectance spectroscopy (UV-Vis DRS), X-ray photoelectron spectroscopy (XPS), Raman spectroscopy, and electron spin-resonance spectroscopy (ESR), with representative results compiled in Figure 2 [24-27]. In UV-Vis DRS, ultraviolet light strikes the TiO_{2-x} sample and the wavelengths and intensities of the scattered component are recorded; Figure 2a shows that Ti^{3+} formation displaces the absorption edge or produces entirely new bands. Bandgaps derived from these data via the Kubelka–Munk function (Figure 2b) fall in the 2.4–2.8 eV range, well below the 3.1 eV of ordinary TiO_2, which indirectly attests to oxygen-vacancy generation[17]. XPS infers the energy-level structure and chemical environments of TiO_{2-x} from photoelectrons expelled by incident X-rays: the Ti^{3+}-associated titanium fraction is resolved in Figure 2c [25], whereas Figure 2d provides a quantitative breakdown of vacancy-related oxygen [26], in which the labels OL, OA, and OW stand for lattice oxygen, oxygen-vacancy species, and adsorbed oxygen, in that order. Raman analysis detects vacancies through shifts in characteristic bands — in Figure 2e, the dominant peak of untreated white TiO_2 (W-TO) moves from 145.2 cm^{-1} to 149.7 cm^{-1}, and such blue-shifted, broadened features are diagnostic of oxygen vacancies[27]. Lastly, because both vacancies and Ti^{3+} contribute electronic states bearing unpaired spins, they register in ESR: Figure 2f [27] assigns the resonance at g=2.001 to oxygen vacancies and that at g=1.946 to Ti^{3+} species located at the TiO_{2-x} surface.

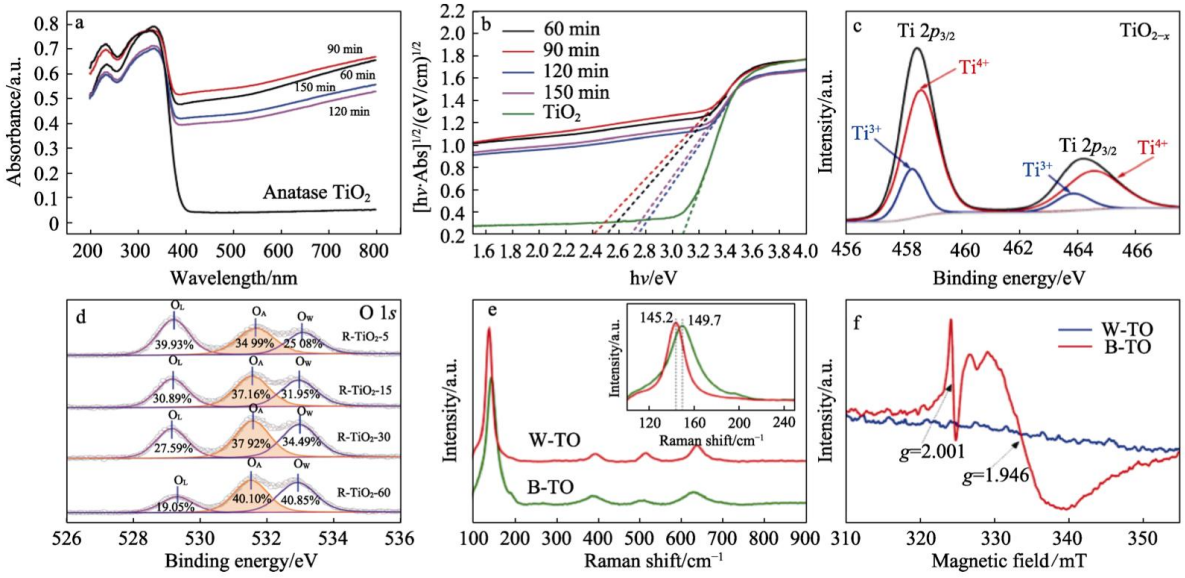

Figure 2 UV-Vis DRS (a, b), XPS (c, d), Raman (e), ESR (f) spectra of TiO2 and TiO2–x[24-27]

In aggregate, the architecture of TiO_{2-x} — a crystalline interior sheathed by a disordered shell rich in oxygen vacancies, Ti^{3+}, and allied defects — works to the advantage of its photocatalytic behavior[28]. Deliberately engineering this structure, however, poses considerable difficulty: no straightforward route yet exists for

choosing a synthesis and adjusting its parameters such that the shell thickness and the vacancy and Ti^{3+} populations of the disordered layer can be set at will. Moving forward, efforts should therefore integrate the characterization techniques described above with judiciously chosen synthesis methods and process parameters, enabling precise structural engineering and, ultimately, the desired photocatalytic performance.

3 Synthetic Methods for TiO_{2-x}

Selection of synthetic strategies for TiO_{2-x} exerts direct impacts on distributions of oxygen vacancies, \(Ti^{3+}\) and magnitudes of forbidden bandgap Eg. TiO_{2-x} can presently be manufactured through several distinct pathways, including high-temperature calcination–reduction, electrochemical processing, and the oxidation of low-valence titanium precursors; each route offers a means of adjusting the material's structural and bandgap characteristics to secure targeted photocatalytic properties.

3.1 High-Temperature Calcination-Reduction Method

High-temperature calcination–reduction works by exposing TiO_2 to a reductant at elevated temperatures, under which Ti^{4+} is transformed into Ti^{3+} and oxygen vacancies are simultaneously created; together these changes compress the bandgap of TiO_{2-x} and invigorate its photocatalytic response. Frequently employed reductants include H_2, $NaBH_4$, Al, Zn, Mg, CaH_2, and imidazole[8,29-39]. Classified by reductant identity, the approach branches into hydrogen reduction, plasma reduction, and assorted other variants; judicious adjustment of temperature, pressure, gaseous environment, and reductant selection grants access to TiO_{2-x} products spanning diverse structural motifs and bandgap values. An overview of the preparation conditions reported for TiO_{2-x} obtained through this route, along with the corresponding bandgap values and principal structural characteristics, is provided in Table 1.

Table 1 TiO_{2-x} Prepared via High-Temperature Calcination-Reduction Routes

Reduction method	Sample designation	Preparation conditions	Eg /eV	Dominant structural features	References
H_2 reduction	TiO_{2-x} nanoparticles	Pure H2, 2 MPa high pressure, 200 ℃, 5 d	1.54	Oxygen vacancies, Ti^{3+}	[8]
	Mesoporous TiO_{2-x} hollow spheres	Pure H2, atmospheric pressure, 600 ℃, 3 h	2.59	Spherical morphology, oxygen vacancies, Ti^{3+}	[29]
	TiO_{2-x} nanoparticles	H2-N2 mixed gas (8 vol% H2), 700 ℃	2.78	Oxygen vacancies, Ti^{3+}	[30]
	TiO_{2-x} nanorod arrays	H2-Ar mixed gas (20 vol% H2), 350 ℃	—	Oxygen vacancies, Ti^{3+}	[31]
Plasma reduction	TiO_{2-x} nanoparticles	Hydrogen plasma, 500 ℃, 8 h	2.05	Amorphous shell layer, oxygen vacancies, Ti^{3+}	[32]
	TiO_{2-x} thin films	H2-Ar plasma, 300 ℃	2.60	Oxygen vacancies, Ti^{3+}	[33]
Other reduction approaches	TiO_{2-x} nanoparticles	Nitrogen atmosphere, sodium borohydride, 350 ℃	2.11	Oxygen vacancies, Ti^{3+}	[34]

	TiO_{2-x} nanoparticles	Vacuum environment, ethanol, 400 ℃, 3 h	1.92	Oxygen vacancies	[35]
	TiO_{2-x} nanoparticles	Nitrogen atmosphere, sodium azide, 450 ℃, 2 h	2.70	Oxygen vacancies, Ti^{3+}	[36]
	TiO_{2-x} nanoparticles	Vacuum environment, aluminum powder, 300-500 ℃, 6 h	—	Spherical morphology, oxygen vacancies, Ti^{3+}	[37]
	TiO_{2-x} nanoparticles	Vacuum environment, elemental potassium, 140 ℃, 1 h	0.45	Disordered surface shell, oxygen vacancies, Ti^{3+}	[38]
	TiO_{2-x} nanoparticles	Imidazole, 350 ℃, 2 h	1.86	Oxygen vacancies, Ti^{3+}	[39]

Note: "—" means not mentioned in corresponding references. Same hereinafter.

The hydrogen-reduction route treats whiteTiO2 under regulated pressure, temperature and holding time. Reductive hydrogen replaces lattice-oxygen atoms to generate oxygen vacancies and yield TiO_{2-x}. CHEN et al.[8] pioneered treating whiteTiO2 for 5 d at 200 ℃ under 2 MPa high-purity hydrogen atmosphere and obtained TiO_{2-x} with a 1.54 eV bandgap. Hydrogen incorporation introduces intermediate energy levels situated between conduction bands and valence bands, narrows forbidden bandgaps and broadens spectral-response ranges. Under identical testing conditions, photocatalytic activity of resultant TiO_{2-x} doubles compared with pristineTiO2. Through a sequence of template-free solvothermal growth, encapsulation with small amine molecules, and hydrogen reduction (ramping to 600 °C at 10 °C/min under atmospheric-pressure H_2 and holding for 3 h), HU et al.[29] obtained hollow-spherical TiO_{2-x} with a bandgap reduced to 2.59 eV. When illuminated by sunlight, it produces hydrogen at 2410 μmol/(h·g) — a rate close to triple that recorded for white TiO_2 (810 μmol/(h·g)). ZHANG et al.[30] reducedTiO2 under flowing 8 vol% hydrogen-nitrogen mixed gas with a flow rate of 50 SCCM (SCCM≈0.00004719L/min similarly hereinafter) at 700 ℃ and prepared TiO_{2-x} with bandgap of 2.78 eV. Under open-circuit conditions, its hydrogen-evolution performance nearly doubles relative to white nano-\(TiO_2\). In the study by ZHANG et al.[31], TiO_2 nanorod arrays were hydrothermally deposited onto fluorine-doped tin-oxide (FTO) glass, after which hydrogenation was carried out by heating the arrays to 350 °C (5 °C/min ramp) in a flowing H_2/Ar blend of 20 and 80 SCCM, respectively. The resulting TiO_{2-x} nanorod arrays were employed as photoelectrodes for the degradation of organic compounds. Light-absorption ranges extend into visible-light domains; absorbance for ultraviolet-light and visible-light regions rises by 4 % and 50 % respectively. For hydrogen-reduction synthetic workflows, tuning hydrogen content, heating ramp rates, reaction temperatures and holding durations enables modulation of hydrogenation degrees forTiO2, which offers guiding significance for determining defect chemical properties. Nonetheless, high costs and safety hazards inherent to this procedure prevent its large-scale industrial deployment.

Hydrogen-plasma treatments are generally executed under vacuum or low-pressure environments, featuring superior safety and environmental compatibility compared with high-pressure hydrogen workflows. WANG et al.[32] treated TiO_2 in a hydrogen plasma at 500 °C over 8 h, producing TiO_{2-x} that captures 83% of incoming solar radiation — a level of absorption credited to localized surface plasmon resonance (LSPR). Since LSPR intensity scales with the density of surface carriers, the process works by implanting hydrogen and/or oxygen vacancies, which convert surface $Ti^{4+}(3d^0)$ into $Ti^{3+}(3d^1)$ and swell the electron concentration. Separately, PYLNEV et al.[33] generated TiO_{2-x} films with a 2.60 eV bandgap by sputtering conductive TiO_2 targets in an H_2/Ar plasma held at 300 °C. Hydrogen-plasma sputtering drives the material through a well-defined structural progression: the anatase XRD signals first broaden, rutile then emerges partially, amorphization follows, and crystalline intermediate titanium oxides ultimately appear. Hydrogen plasma delivers high-energy input, shortens reaction durations and proves more suitable for large-volume high-quality material fabrication compared with direct

hydrogen-gas utilization.

Hydride reagents or other safer reducing agents can also be exploited for synthesizing TiO_{2-x} . ARIYANTI et al.[34] produced TiO_{2-x} by combining TiO_2 powder with $NaBH_4$ and firing the mixture in an argon-flushed furnace at temperatures between 300 and 450 °C. This material achieves complete degradation of rhodamine B (RhB) within 50 min, whereas conventionalTiO2 consumes over 90 min for equivalent degradation. CHEN et al.[35] utilized ethanol as reducing agent under vacuum conditions, reacted for 3 h at 400 ℃ and generated TiO_{2-x} with bandgap equal to 1.92 eV. Benchmarked side by side, the resulting TiO_{2-x} nanoparticles decompose methylene blue (MB) at 1.8 times the rate of their untreated counterparts; interestingly, ethanol-reduced samples exhibit no discernible Ti^{3+}, implying that oxygen vacancies on their own function as mid-bandgap traps restraining electron–hole recombination. ZHENG et al.[36] turned to sodium azide (NaN_3), reacting it with TiO_2 at 450 °C for 2 h in nitrogen; the product absorbs across the whole solar spectrum and evaporates water at 1.624 kg/(m^2·h), dwarfing the 0.515 kg/(m^2·h) of white TiO_2. In WANG et al.'s study[37], molten aluminum acted as the oxygen scavenger: commercial white TiO_2 was processed into TiO_{2-x} within a dual-zone tube furnace run at 300–500 °C (schematic in Figure 3), the driving step being Al's extraction of lattice oxygen from pre-annealed TiO_2, which seeds oxygen vacancies (OV) throughout the bulk; relative to the parent oxide, the Al-reduced material harvests some 60% additional solar energy. A far more aggressive narrowing was reported by LIN et al.[38], who reduced TiO_2 with elemental potassium under vacuum at 140 °C for 1 h, yielding TiO_{2-x} with a mere 0.45 eV bandgap and a visible-light MB-degradation rate more than 300 times that of white TiO_2. AZAB et al.[39] pursued yet another chemistry: TiO_2 and imidazole were combined at 1:2 by mass, 3 mL of 37 wt% HCl was introduced, and the blend was fired in a muffle furnace — first to 350 °C (5 °C/min, 2 h hold), then 400 °C for a further hour — giving TiO_{2-x} with a 1.86 eV bandgap. Common to all such chemical-reduction approaches is that the reductant dosage, processing temperature, and reaction time collectively shape the final photocatalytic outcome. Avoidance of hydrogen-gas deployment renders these convenient, mild approaches for manufacturing TiO_{2-x} powders and thin-film specimens.

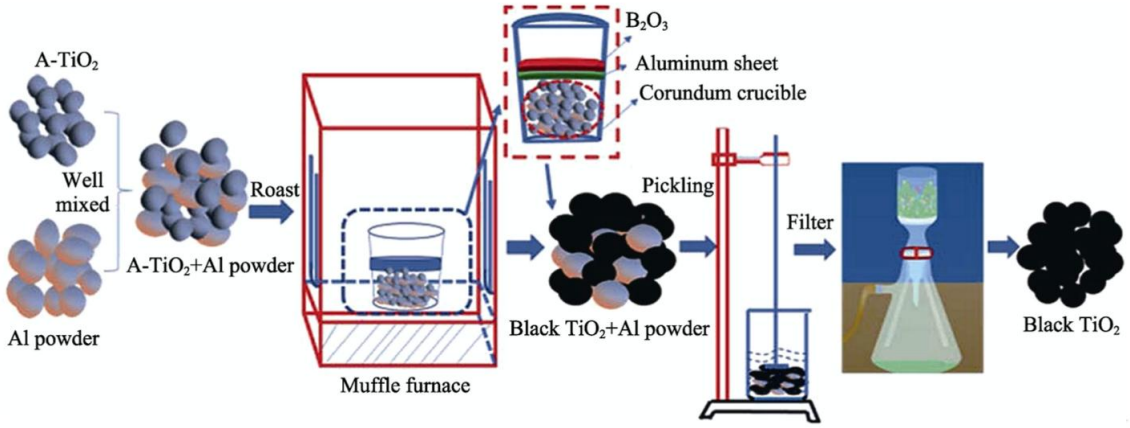

Figure 3 Schematic diagram of TiO2–x synthezed by aluminum thermal reduction[37]

On the whole, conventional hydrogen-reduction procedures call for high temperatures coupled with extended reaction periods; raising the temperature, while accelerating the hydrogen reaction and altering the defect landscape of the product, simultaneously inflicts damage on the material's framework. Moreover, increased hydrogen concentrations trigger lattice expansion and nanoparticle-size shrinkage, culminating in narrowed bandgap magnitudes. When compared against conventional hydrogen-reduction protocols, hydrogen-plasma-reduction procedures dispense with extra catalysts or solvents. Benefiting from LSPR effects, they improve light-absorbing and photodegradation capabilities. Nevertheless, excessive cost restricts large-scale production for both above-mentioned methodologies. Syntheses of TiO_{2-x} relying on alternative reducing agents (e.g. $NaBH_4$, NaN_3) generally entail liquid-phase processing or solid-phase grinding to achieve homogeneous mixing. Different reducing-agent species induce distinct defect patterns within final materials. In general, hydride-based and other alternative reductant routes proceed under gentle conditions, imposing little environmental load while offering high efficiency, modest energy demand, and short processing times. Mechanistically, the formation of TiO_{2-x} through these approaches proceeds along two distinguishable routes.

First, reductants such as H2, ethanol or imidazole directly undergo displacement reactions withTiO2 under high-temperature environments, enabling titanium atoms to capture electrons and become reduced. Second, powerful reducing substances decomposed at high-temperature conditions (for instance H2, elemental sodium) reduceTiO2, as exemplified by $NaBH_4$, and NaN_3.

3.2 Electrochemical-Synthesis Method

Most electrochemical strategies employ titanium foil as the starting material: an impressed voltage oxidizes the foil anodically in solution, building TiO_2 nanotubes laden with defects, and a concluding heat treatment transforms them into TiO_{2-x}. QI et al.[40] configured a titanium foil as the anode opposite a platinum cathode; following 1 h of anodization, the assembly was annealed at 450 °C for 2 h (5 °C/min ramp) to establish the photoelectrode, and a subsequent 30 min electrochemical reduction injected Ti^{3+} and oxygen vacancies — the outcome being TiO_{2-x} with a 2.7 eV bandgap whose sensitivity extends well into the visible. In the alternative procedure of LI et al.[41], titanium sheets underwent 1 h of anodization at 60 V against platinum coils in an ethylene-glycol bath formulated with 0.05 mol/L ammonium fluoride (NH_4F); successive washing in distilled water and ethanol, drying, and a final 24 h soak at 60 °C delivered TiO_{2-x} displaying a bandgap of 2.71 eV. Electrodes constructed from this material deliver photocurrent density reaching \(91.7\ \mathrm{\mu A/cm^2}\), nearly four times higher than anodized white-TiO2 counterparts. Such electrochemical-synthesis workflows can manufacture TiO_{2-x} within relatively short time spans. Precise adjustment of current intensities and deposition durations grants effective control over product thickness and morphology, affording favorable controllability and reproducibility.

3.3 Oxidation Method Using Low-Valent-Titanium Compounds

The low-valent-titanium-compound oxidation method employs raw materials bearing low-valence titanium atoms including metallic Ti, TiH_2 and TiO. Ti^{3+} or H^+ species get doped into crystal lattices to form core-shell-structured TiO_{2-x} with disordered outer surfaces. In the approach reported by LIU et al.[42], titanium hydride (TiH_2) was combined with hydrogen peroxide, producing a yellow-green gel. After drying, specimens were heated under argon-gas flow of 20 mL/min with 5 ℃/min heating ramp and produced TiO_{2-x} . Relative toTiO2, as-synthesized TiO_{2-x} displays strong absorbance across 400-800 nm visible-light spectrum. Its photocatalytic methylene-blue degradation performance surpasses commercialTiO2 by a factor of 68. REDDY et al.[43] annealedTiO2 for 25 min at 450 ℃ under high-oxygen flow rate of 5 L/min and obtained thermally stable TiO_{2-x} . Although oxidation of low-valent-titanium precursors expands material options for preparation workflows, impurity contamination may arise throughout oxidation steps and requires removal, which inevitably elevates manufacturing complexity and costs.

3.4 Other Innovative Synthetic Approaches

Alongside deepening research efforts, multiple innovative synthetic routes keep emerging. SU et al.[44] adopted pulsed-laser irradiation treatment, scanningTiO2 surfaces at scan speed of 10 mm/s. Sample color transitions from white toward black, accompanied by drastically enhanced absorption within visible-light and near-infrared spectral domains. During pulsed-laser exposure, high-energy laser beams interact withTiO2 target surfaces and induce localized high-temperature events. Lattice-oxygen atoms escape under such thermal inputs to produce oxygen vacancies and boost photocatalytic performances. JEDSUKONTORN et al.[45] reduced metallic titanium via electric-spark synthesis, fabricating TiO_{2-x} under 20 kHz electric-spark pulse frequency and 2 μs pulse width, achieving minimum bandgap value of 2.44 eV. Investigations reveal that light-absorption magnitudes gradually rise as ultrasonic-processing durations increase. Inside electric-spark machining procedures, electrode discharges generate high temperature and high pressure, breaking chemical bonds overTiO2 surfaces and generating oxygen vacancies. RAES et al.[46] implemented sonochemical synthesis with power density of 8000 W/L and subjectedTiO2 to sonication treatments of varied durations. Powder color progressively deepens with extended sonication durations, as shown in Figure 4. This phenomenon originates predominantly from sonochemical cavitation effects, which shift light-absorption wavelengths toward longer wavelengths. After 7 h sonication treatment, resultant photocatalytic activity doubles.

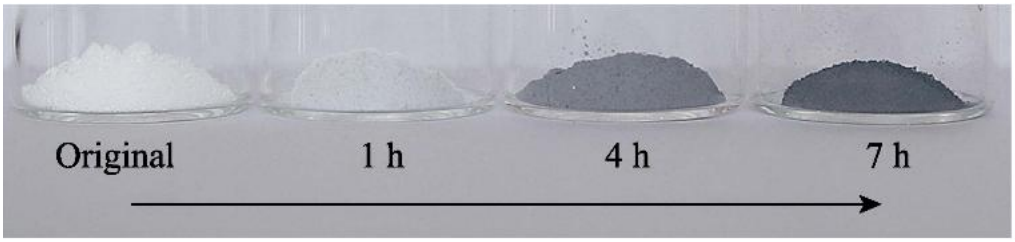

Figure 4 Color variation of TiO2–x prepared by ultrasonic synthesis method with time[46]

Weighing the mechanistic foundations against practical advantages and shortcomings reveals clear trade-offs: calcination–reduction at elevated temperatures exacts a heavy energy toll and unwieldy operations; electrochemical methods cannot furnish powdered TiO_{2-x}; and pulsed-laser processing carries prohibitive equipment costs. The principles, benefits, and weaknesses of these four families — high-temperature calcination–reduction, electrochemical synthesis, low-valent-titanium-compound oxidation, and other novel approaches — are juxtaposed in Table 2. Moreover, identifying suitable, efficient synthetic protocols for heavily-defected TiO_{2-x} deployed in diverse practical domains poses certain challenges. Hence, exploring facile, safe, energy-saving, high-efficiency and universal synthetic strategies, as well as designing surface-defect introduction and precise tuning of morphology and particle sizes targeted for specific application scenarios, constitute key directions for upcoming investigations.

Table 2 Process Comparison of Synthetic Approaches for TiO_{2-x}

Methods	Synthetic principle	Advantages and disadvantages	References
High-temperature calcination-reduction	TiO_2 receives reduction treatments under high-temperature circumstances. Calcination temperature, holding time and atmosphere conditions are regulated. Ti^{4+} gets reduced to Ti^{3+} and defects such as oxygen vacancies are generated.	Advantages: relatively mature preparation procedures. Disadvantages: high-energy consumption, complicated operations, poor controllability over product morphology and performances, difficulties for industrial-scale production.	[8,29-38]
Electrochemical synthesis	External voltages are exerted inside electrolyte solutions, triggering anodic-oxidation reactions upon titanium-sheet substrates to produce TiO_{2-x}.	Advantages: mild reaction conditions, good controllability, suitable for high-purity TiO_{2-x} preparation. Disadvantages: large equipment investment, high costs; preparation efficiency constrained by electrode materials and electrolysis parameters; incapable of reducing powdered TiO2.	[40-41]
Low-valent-titanium -compound oxidation	Oxidize low-valence-titanium-containing compounds to synthesize \(Ti^{3+}\)-bearing TiO_{2-x}.	Advantages: abundant raw-material sources, mild reaction conditions, applicable for powder and thin-film manufacturing. Disadvantages: by-products may be formed throughout oxidation procedures, compromising	[42-43]

		product purity and performances.	
Other innovative synthetic routes	Localized high-temperature conditions prompt lattice-oxygen-atom escape and produce oxygen-vacancy-containing TiO_{2-x} .	Advantages: fast reaction speed, high product purity. Disadvantages: stringent equipment requirements, large-energy consumption; thin-film manufacturing still awaits further exploration.	[44-46]

4 Modification Strategies for TiO_{2-x}

Even though TiO_{2-x} surpasses conventionalTiO2 with respect to light-absorption capabilities and photocatalytic performances, bare TiO_{2-x} delivers mediocre practical performances. In pursuit of heightened activity and robustness, TiO_{2-x} can be further refined through measures such as anchoring metal nanoparticles, incorporating non-metal dopants, erecting heterojunctions, or integrating it with adsorbent supports — each helping to tune its properties toward the demands of particular reaction environments.

4.1 Metal Loading

Loading metallic nanoparticles leverages surface plasmon resonance (SPR) effects and facilitates photogenerated-charge separation to enhance photocatalytic performances. Its mechanistic schematic is displayed in Figure 5a[47]. Part of the photoexcited electron population is diverted toward the Cu co-catalyst, which lowers the odds of electron–hole recombination. BI et al.[48] first fabricated TiO_{2-x} through dual-zone aluminum reduction and subsequently anchored gold nanoparticles (Au NPs) onto it via an adapted deposition–precipitation method; the resulting material combines a vacancy-rich surface with greatly expedited separation and transfer of photogenerated carriers. Visible-light tests (Figure 5b) demonstrate the difference starkly: Au/TiO_2 manages a phenylacetylene conversion of merely 3.2%, while Au/TiO_{2-x} attains 43.1%. Along similar lines, CONG et al.[49] immersed TiO_{2-x} in silver-nitrate solution under UV-Vis exposure, and the stirring–washing sequence that followed produced silver-bearing substrates (\(Ag/b-TiO_2\)); compared with conventionally loaded Ag/TiO_2, these exhibit heightened sensitivity, achieving rhodamine-6G detection down to 1×10^{-12} mol/L (Figure 5c). YUAN et al.[50] resorted to impregnation to fix isolated ruthenium atoms onto hydrogen-plasma-synthesized TiO_{2-x}, yielding Ru/TiO_{2-x} (Figure 5d); the hydrogen-evolution rate consequently leapt from 0.38 mmol/(g·h)) for the bare oxide to 17.81 mmol/(g·h) (all rates normalized to catalyst mass). DFT modeling complemented by photoelectrochemical analysis traces this enhancement to Ru-induced impurity states, which capture charges and smooth the path for electron separation and migration. The same group[51] later combined $PdCl_2$ with TiO_2 ultrasonically in an acidic medium before $NaBH_4$ reduction, producing Pd/TiO_{2-x}; relative to Pd/TiO_2, this catalyst (Figure 5e) delivers superior activity, a diminished overpotential, and a larger limiting current — improvements credited mainly to surface plasmon resonance coupled with palladium-derived synergy. Separately, ZHANG et al.[47] built a series of Cu/TiO_{2-x} photocatalysts by photoinduced deposition from copper nitrate; beyond its co-catalytic role in curbing carrier recombination, copper supplies the active centers at which CO_2 is photoreduced to hydrocarbons, and the top-performing Cu-decorated samples release CH_4 and C_2H_4 at maximum rates of 9.9 and 4.8 μmol/(g·h), respectively (Figure 5f). Collectively, these cases underscore the decisive contribution of metal-nanoparticle decoration to TiO_{2-x} photocatalysis: carrier separation and transfer quicken, overall efficiency climbs, and metals spanning Au, Ag, Ru, Pd, and Cu additionally furnish fresh trapping sites while invigorating the catalytic function of the host material.

DOI:

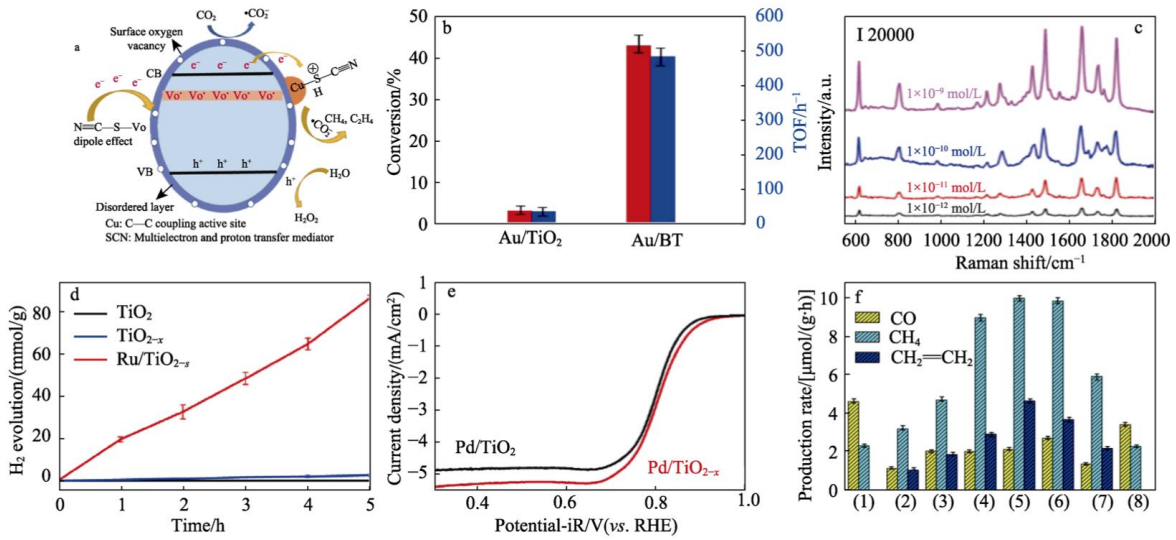

Figure 5 Schematic diagram of mechanism of metal load (a) and performance comparison of Au load (b), Ag load (c), Ru load (d), Pd load (e) and Cu load (f)[47-51]

4.2 Non-Metal Doping/Composite Construction

Doping TiO_{2-x} with non-metallic elements reshapes its electronic structure, extending the range of absorbed wavelengths, contracting the bandgap, and in turn boosting its photocatalytic performance. YANG et al.[52] heated aluminum-reduced TiO_{2-x} for 4 h under sulfur-containing atmospheres, enabling sulfur incorporation into oxygen-deficient shells ofTiO2. As-obtained R'-TiO2-S exhibits drastically enhanced absorbance within visible-light and near-infrared domains, with bandgap reduced down to 0.6 eV. According to Figure 6a, sulfur-doped anatase TiO_{2-x} R'-TiO2-S achieves nearly complete degradation of methyl orange (MO) within 4 h, whereas whiteTiO2 R-TiO_2 scarcely produces degradation effects. Sulfur dopants operate as electron traps capturing photogenerated electrons from TiO_{2-x} and accordingly facilitate separation of photogenerated electron-hole pairs.

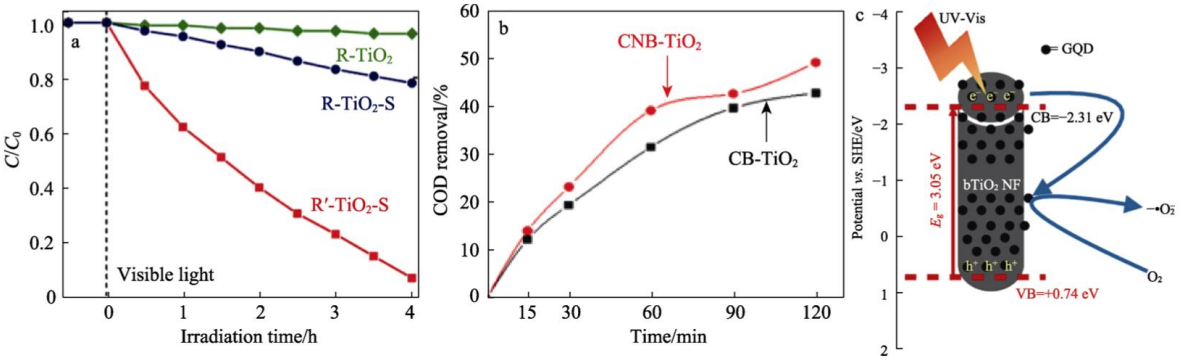

Figure 6 Properties comparison of non-metallic S-doped (a) [52], C and N-doped (b) [53] , and schematic diagram of mechanism of black TiO2 nanofiber (bTiO2 NF)-graphene quantum dot composites (c)[54]

RAHMAN et al.[53] first hydrolyzed TiCl4 inside glycerol-containing aqueous solutions to produce Ti(OH)4 colloids. The carbon-doped derivative BTiO2 was realized by spiking the colloidal suspension with ammonium hydroxide and firing at 300 °C for 1 h, whereas metered addition of urea to the precursor sol yielded the carbon–nitrogen co-doped counterpart CNB-TiO2. Each variant performs creditably in photocatalysis (Figure 6b), registering narrowed bandgaps of 2.63 eV and 2.06 eV, respectively. Dopant carbon and nitrogen insert fresh states into the forbidden gap of TiO_{2-x} — shrinking it — and additionally operate as electron donors or acceptors that furnish

extra charge carriers, thereby lifting catalytic efficiency. A further avenue for enhancement lies in marrying TiO_{2-x} to graphene quantum dots (GQD): SHAFIEE et al.[54] reduced TiO_{2-x} chemically and then co-dispersed it with GQD under ultrasonication, obtaining GQD-TiO2-x hybrids whose bandgap, notably, expands from 2.36 eV to 3.05 eV (Figure 6c). Acting as a co-catalyst, GQD channels absorbed light energy toward TiO_{2-x} and thus improves photon utilization, while also generating reactive species on its own; at the same time, the heterointerfaces established between GQD and the photocatalyst reinforce electron–hole separation, collectively delivering superior photocatalytic efficiency. Given outstanding performances delivered by non-metal-doped TiO_{2-x} , upcoming research ought to focus upon precise modulation of doping categories, concentrations and doping modalities to further optimize TiO_{2-x} performances and extend its applicability across additional domains[55-56].

4.3 Heterojunction Construction

Rationally designed TiO_{2-x} heterojunction architectures suppress photogenerated-electron-hole-pair recombination across heterointerfaces and optimize electron-transport pathways for elevated catalytic activities, preserving satisfactory performances even under long-duration high-efficiency operational circumstances. CUI et al.[57] fabricatedTiO2/indium-oxide S-scheme heterojunctions 10-B-TiO_2/In_2O_3 featuring three-dimensional porous inverse-opal architectures. Investigations reveal that these heterojunction catalysts deliver CO production rate reaching 162.5 mmol/(g·h), which is 1.6-fold higher than that of white-counterpart heterojunctions, as illustrated in Figure 7a. Electrons transfer from conduction bands of TiO_{2-x} across heterojunction interfaces into valence bands of In_2O_3, generating space-charge regions. This arrangement shepherds photogenerated electrons and holes apart swiftly, so the resulting materials combine broad full-spectrum sensitivity with fast carrier separation and migration, underpinning excellent photocatalytic performance. Moreover, as a newly developed heterojunction paradigm, the S-scheme layout safeguards the potent redox capability that photocatalytic transformations demand.

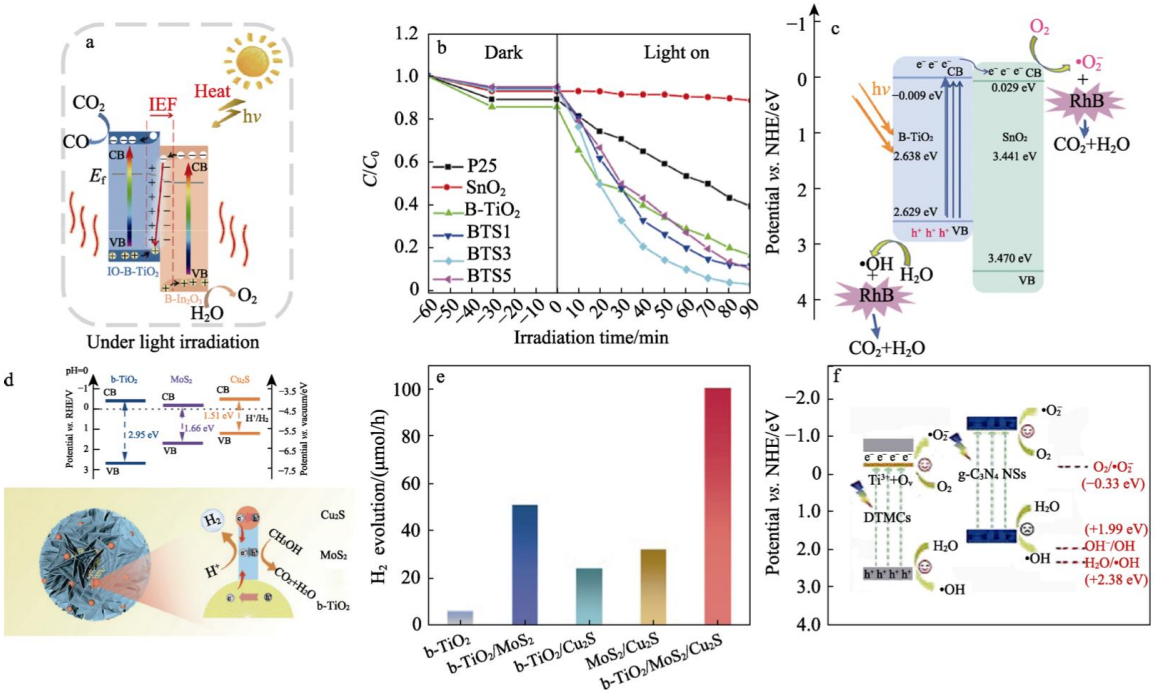

Figure 7 Schematic diagram of S-type heterojunction (a)[57] photocatalytic performance (b) and schematic diagram of type II heterojunction (c) [58] , schematic diagram of hierarchical tandem heterojunction (d) and its hydrogen evolution rate (e) [59] and schematic diagram of photocatalytic mechanism Z-type heterojunction (f)[60]

LI et al.[58] adopted chemical synthetic routes to couple tin-oxide SnO2 with magnesium-thermally-reduced TiO_{2-x} and prepared type-II heterojunctions abbreviated BTS. Figure 7b shows that specimen BTS3 achieves maximum RhB degradation efficiency up to 96.62 %, while bare TiO_{2-x} merely attains 80 % RhB degradation rate.

Its photocatalytic-mechanism schematic is presented in Figure 7c. Since conduction-band potential for SnO2 (0.029 eV) sits lower than that of TiO_{2-x} (-0.009 eV), photogenerated electrons located on conduction bands migrate onto conduction bands of SnO2. Accordingly, synergistic effects originating from type-Ⅱ heterojunctions effectively strengthen separation capacities for photogenerated electron-hole pairs and accelerate transportation efficiencies for photogenerated charge carriers. Through a solvothermal route, LI et al.[59] grew MoS2 and Cu2S nanoribbons on the surfaces of high-temperature-calcined TiO_{2-x} microspheres, thereby assembling hierarchical tandem heterojunctions of TiO2-x/MoS2/Cu2S (Figure 7d). TiO_{2-x} serves as favorable electron-donating material; narrow-bandgap Cu2S (1.51 eV) constitutes outstanding light-absorbing and electron-supplying substance; MoS2 operates as electron-accepting material and charge-transport channel, which collectively broaden light-absorption windows for entire heterojunction systems. According to Figure 7e, hydrogen-evolution rates for TiO2-x/MoS2/Cu2S reach as high as 101.3 μmol/h, vastly exceeding values measured for bare TiO_{2-x} . TAN et al.[60] exploited g-C3N4 as a growth template upon which defect-tailored TiO_{2-x} crystallites were assembled into intimate junctions, successfully establishing Z-scheme TiO2-x/ g-C3N4 composite systems. Experimental results indicate that such heterojunctions achieve superior methyl-orange degradation ratios compared with bare TiO_{2-x} nanoparticles DTMCs. As demonstrated in Figure 7f, photogenerated electrons residing within conduction bands of DTMCs directly recombine with holes located within valence bands (VB) of g-C3N4 across heterointerfaces. This arrangement greatly facilitates the dissociation of photogenerated electrons from holes, translating into stronger photocatalytic activity. More broadly, building heterojunctions brings together disparate lattice structures and band alignments, which hasten electron-transfer kinetics and augment light capture — together delivering enhanced photocatalytic performance.

4.4 Compositing with Adsorptive Materials

Materials like activated carbon, biochar produced from coconut shells, and naturally occurring kaolinite see broad use in pollution remediation, prized for their exceptional ability to capture contaminants. Their combination of good electrical conductivity, generous surface area, and environmental friendliness also renders them excellent platforms on which to build high-performance photocatalytic hybrids. Nevertheless, TiO_{2-x} as photocatalytic material suffers from tiny particle dimensions, severe particle-agglomeration tendencies, low electron-hole-pair-separation efficiencies and unsatisfactory cyclic stabilities. To overcome these drawbacks, TiO_{2-x} gets composited with adsorptive materials to generate innovative composite systems possessing synergistic adsorption-photocatalysis functions. Incorporation of adsorptive substrates, on one hand, substantially elevates photogenerated-electron-transfer efficiencies for TiO_{2-x} and lowers recombination rates for electron-hole pairs. On the other hand, adsorptive materials with large specific-surface-area values supply abundant adsorption sites, facilitating contact efficiencies between pollutants and photocatalysts and thereby accelerating photocatalytic-reaction rates. Additionally, acting as supporting carriers, adsorptive substrates effectively mitigate particle-agglomeration phenomena for TiO_{2-x} and enhance material dispersion and stability. LI et al.[61] adopted sol-gel methodologies, stirred pre-treated activated carbon (AC), absolute ethanol, tetrabutyl titanate and glacial acetic acid in appropriate proportions to produce transparent hydrogels. After drying and grinding, calcination treatments were implemented at 500 ℃ to synthesize \(TiO_{2-x}/AC\) composite materials. Rhodamine-B degradation efficiencies improve by over 20 % (Figure 8a). From Figure 8b, activated-carbon components furnish electron-transport pathways and suppress carrier-recombination rates, delivering far superior photocatalytic degradation capacities relative to standalone AC or bare TiO_{2-x} . As illustrated in Figure 8c, photocatalytic performances manifest no conspicuous deterioration after four consecutive recycling cycles, because TiO_{2-x} immobilized over AC surfaces gains improved dispersity and stability. ZAKARIA et al.[62] dispersed TiO_{2-x} , TiN and coconut-shell-derived biomass carbon (ACB) at mass ratio 1∶1∶5 separately within 50 mL ethanol solutions and stirred for 2 h, followed by calcination treatments to fabricate \(TiO_{2-x}/TiN@ACB\) composites. Mutual reinforcement between ACB and the TiN/TiO_{2-x} phases facilitates the swift parting and shuttling of photogenerated carriers, and — as evidenced in Figure 8d — the resulting composites exhibit substantially heightened catalytic performance coupled with remarkable long-term stability. indeed, Figure 8e shows that after three consecutive reuse cycles, the loss of performance does not exceed 3%. In a related study, HU et al.[63] fabricated TiO_{2-x} composites modified with natural kaolinite through a hydrothermal process, and the resulting materials eliminated methylene blue completely (100% removal), a dramatic improvement over the mere 32% achieved by unmodified TiO_{2-x}. As presented in Figure 8f, porous composite architectures obtained after kaolinite modification for TiO_{2-x} firmly anchor TiO_{2-x} onto kaolinite surfaces via Al(Si)O-Ti chemical linkages. This modification enhances particle dispersion and multiplies active

centers for TiO_{2-x} .

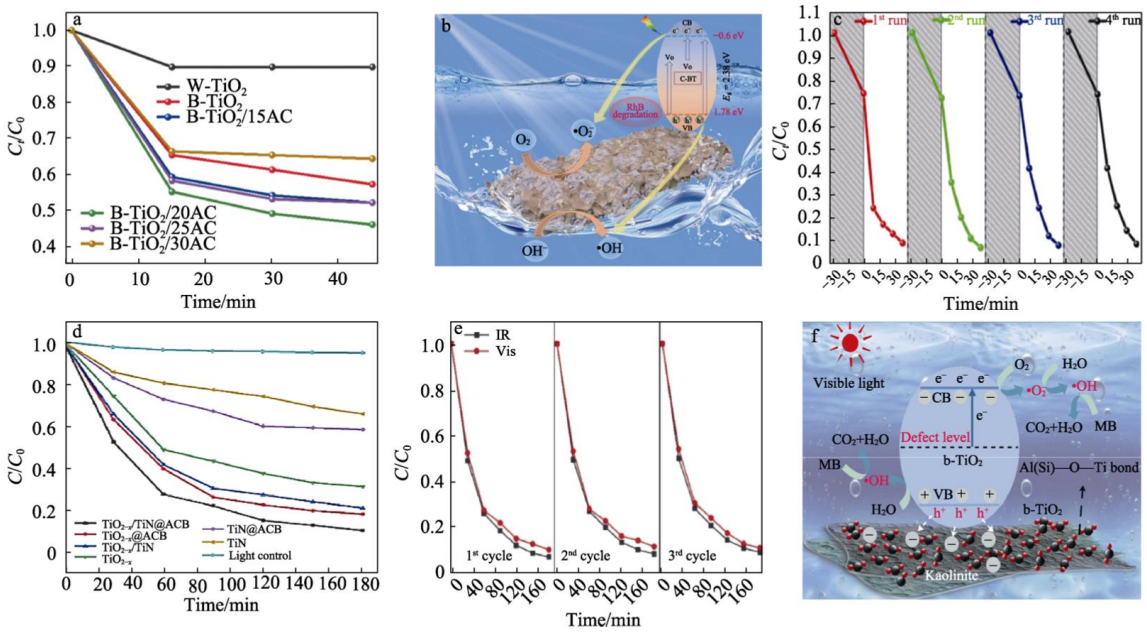

Figure 8 Photocatalytic properties (a), mechanism (b) and number of cycles (c) of TiO2–x/AC composites[61]; Photocatalytic performance (d) and number of cycles (e) of TiO2–x/TiN@ACB[62]; Schematic diagram of mechanism of action of kaolinite-modified TiO2–x (f)[63]

To sum up, compositing adsorptive substrates with TiO_{2-x} can appreciably ameliorate photocatalytic performances of TiO_{2-x} . Electrical conductivity and large specific-surface-area values originating from adsorptive components effectively boost separation efficiencies for photogenerated electrons and holes, meanwhile resolving particle-agglomeration drawbacks of TiO_{2-x} . These properties grant adsorption-photocatalysis synergistic composite materials promising application prospects for elimination of aquatic contaminants.

5 Applications and Mechanisms for TiO_{2-x} and Its Composites in Photocatalytic Degradation of Water-Borne Pollutants

Photocatalytic degradation of water pollutants proceeds without generating secondary contaminants and represents an environmentally benign disposal technology. Overcoming the inherent restriction of conventional TiO_2 to ultraviolet excitation, TiO_{2-x} and its hybrid derivatives harvest light across the full spectrum and accomplish impressive removal of diverse waterborne contaminants — dyes, phenolics, pharmaceuticals, and beyond.

5.1 Degradation of Dyes

MB, RhB, MO, and kindred dyes are manufactured and used on a massive scale in both consumer goods and industrial operations; once such compounds escape into wastewater streams unchecked, they imperil public health and ecological systems. Against this backdrop, harnessing TiO_{2-x} to photocatalytically dismantle dye pollutants presents a remediation strategy that is at once potent and benign to the environment[64-65].

Figure 9 provides a schematic account of this process. On unmodified TiO_{2-x}, the destruction of dyes proceeds stepwise: photons are first harvested, electron–hole pairs are then spawned, oxidizing radicals ensue, and the dye molecules are finally torn apart. Specifically, irradiation at matching wavelengths lifts valence-band electrons (e^-) of TiO_{2-x} into its conduction band, leaving holes (h^+) in their wake; the separated carriers go on to react with hydroxyl ions (OH^-) adsorbed at the surface and with dissolved O_2, giving rise to the powerfully oxidizing hydroxyl (•OH) and superoxide (O_2^-) radicals. These radical species assail dye molecules through addition, substitution,

and electron-transfer pathways, chopping them into small organic fragments that are ultimately converted into inorganic matter; whatever the identity of the dye, the degradation obeys the general logic of redox reactions even though the intermediates differ from case to case[66]. Several investigations exemplify this capability. ZHAI et al.[67] grew highly active porous TiO_{2-x} coatings via suspension plasma spraying, removing 89% of a 5 mg/L methylene-blue solution under visible light. CHEN et al.[68] prepared TiO_{2-x} through ethanol-facilitated reduction beneath a UV lamp, achieving near-total decomposition of 4×10^{-5} mol/L RhB after 65 min of ultraviolet exposure. SAENSOOK et al.[69], working with TiO_{2-x} from high-temperature calcination–reduction, recorded methyl-orange removal of 71.92% in visible light, rising to 82.17% under UV irradiation. Besides, composite materials derived from TiO_{2-x} also deliver remarkable performances for dye-degradation purposes.

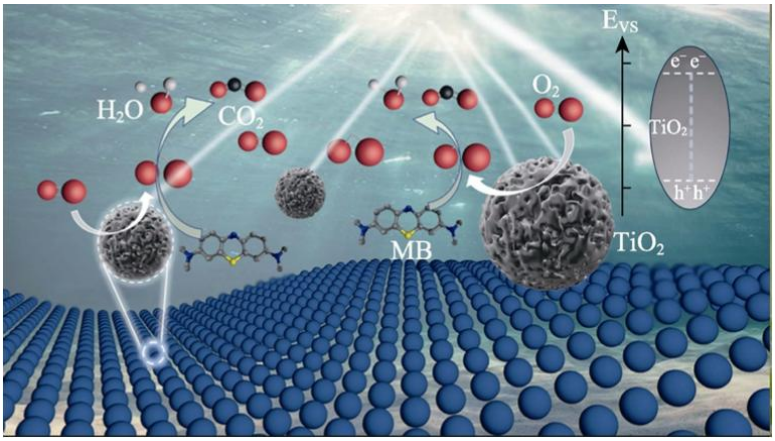

Figure 9 Schematic diagram of TiO2–x photocatalytic degradation of MB

Photocatalytic dye-degradation mechanisms for heterojunction-constructed systems are predominantly rooted in photocatalytic reactions plus performance-enhancement effects originating from heterojunction architectures. YUAN et al.[70] adopted solvothermal-synthesis protocols and prepared N-doped TiO_{2-x}/g-C_3N_4tri-phase heterojunctions N-Ti^{3+}-TiO_2/g-C_3N_4. Under visible-light illumination, it achieves 81 % degradation efficiency for 5 mg/L methylene-blue solutions within 100 min. Ti^{3+} generates intermediate energy levels near conduction-band bottoms of TiO_2, while nitrogen-doping introduces impurity energy levels above valence bands ofTiO2. Photogenerated electrons can get excited from valence bands of TiO2 or 2p energy levels of nitrogen toward Ti^{3+} energy states. Consequently, photoexcited electrons depart g-C_3N_4. and enter the conduction band of the N/ Ti^{3+} co-doped tri-phase structure with greater ease, and the ensuing •OH and O_2^{-1} species act as the primary oxidizers driving MB breakdown. Separately, CHEN et al.[71] illuminated a mixture of $AgNO_3$ and TiO_2 with a 500 W xenon lamp, constructing Ti^{3+}-self-doped Ag_2O/TiO_2 p–n nano-heterojunctions; within 150 min of visible irradiation, these junctions decomposed over 90% of an initially 10 mg/L RhB solution. Here Ag_2O plays the p-type partner while TiO_{2-x} furnishes the n-type phase: electron flow from the n-side to the p-side persists until the Fermi levels coincide, generating an internal electric field that expedites carrier separation and, accordingly, reinforces RhB photodegradation.

Photocatalytic mechanisms for composite systems assembled from TiO_{2-x} and adsorptive materials rest upon extra electron-transport channels or reaction-active sites supplied by adsorptive components, which facilitate photogenerated-electron-hole-pair separation and suppress their recombination, hence elevating dye-molecule-degradation capabilities. WANG et al.[72] united TiO_{2-x} with reduced graphene oxide (RGO) in a solvothermal synthesis, and the resulting hybrid eradicated a 40 mg/L methylene-blue solution completely within 120 min under visible light; mechanistically, electrons promoted into the TiO_{2-x} conduction band drain onto the RGO sheets, fostering carrier separation, whereas •OH and h^+ shoulder the oxidative work of MB removal. Via a sol–gel route, LI et al.[73] fabricated T TiO_{2-x}/AC, which broke down 92% of a 2 mg/L RhB solution over the course of 60 min of visible-light illumination. Activated carbon acts as favorable electron-transfer channel enabling fast electron migration and substantially improving photocatalytic performances; •OH and O2 constitute major reactive species degrading RhB. Table 3 summarizes recent-year performances for TiO_{2-x} alongside diverse composite variants deployed for dye-degradation applications.

Table 3 Performance Comparison for TiO_{2-x} and Its Modified Composites for Dye-Pollutant Elimination

Photocatalyst category	Photocatalyst designation	Synthesis method	Dye pollutant and concentration	Degradation performance	Dominant reactive species	References
Bare TiO_{2-x}	H^-TiO_2	Hydrogen-gas reduction	MB, mass concentration 10 mg/L	90 % degradation within 150 min	—	[74]
	Blue TiO_2	Chemical reduction	MO, mass concentration 15 mg/L	100 % degradation within 90 min	•OH, O_2^-, h^+	[75]
	H-TiO_2	Hydrogen-plasma reduction	RhB, mass concentration 3 mg/L	100 % degradation within 120 min	O_2^-, •OH	[76]
	Ti^{3+} self-dopedTiO2	Low-valent-titanium oxidation	MB, concentration 0.5 mol/L	100 % degradation within 20 min	•OH, O_2^-	[77]
	TiO_{2-x} coating	Suspension plasma-spraying	MB, mass concentration 5 mg/L	89 % degradation within 5 h	—	[63]
	Ti^{3+} self-doped TiO_2	Sonochemical synthesis	RhB, concentration 0.01 mmol/L	100 % degradation within 120 min	•OH, O_2^-	[78]
Non-metal-doped	b-N-TiO_2	Solvothermal synthesis	RhB, mass concentration 3 mg/L	100 % degradation within 160 min	•OH, O_2^-	[79]
	R'-TiO_2-S	Chemical reduction	MO, mass concentration 10 mg/L	100 % degradation within 45 min	•OH, O_2^-	[52]
Metal-loaded	b-Ni-TiO_2	Chemical reduction	MO, mass concentration 10 mg/L	95 % degradation within 150 min	•OH, O_2^-, H_2O_2	[80]
	b-Zr-TiO_2	Solvothermal synthesis	RhB, mass concentration 10 mg/L	95.25 % degradation within 120 min	—	[81]
Heterojunction	N-Ti^{3+}-TiO_2/g-C_3N_4	Solvothermal synthesis	MB, mass concentratio	81 % degradation within	•OH, O_2^-, h^+	[70]

			n 5 mg/L	100 min		
	TiO_{2-x} /g-C_3N_4	Solvothermal synthesis	MO, mass concentration 10 mg/L	96.8 % degradation within 80 min	•OH, O_2^- , h^+	[60]
Composited with adsorptive materials	TiO_{2-x} /AC	Sol-gel method	RhB, mass concentration 2 mg/L	92 % degradation within 60 min	O_2^- , h^+	[61]
	TiO_{2-x}/TiN@ACB	Solvothermal synthesis	MB, mass concentration 10 mg/L	100 % degradation within 120 min	•OH, O_2^-	[63]

Note: Discolored titania variants including H-TiO_2 and BlueTiO_2 all belong to TiO_{2-x} .

5.2 Degradation of Phenolic Compounds

Effluents from petrochemical plants, textile-printing operations, and pesticide production frequently contain phenolic pollutants, whose high solubility in water and pronounced mobility allow them to spread readily; beyond certain concentration limits, they become acutely toxic to living organisms. Employing TiO_{2-x} and its composite derivatives to break down such compounds offers distinct advantages, namely high treatment efficiency, freedom from secondary pollution, and modest energy demand[82].

NAWAZ et al.[83] employed a glycerol-assisted solvothermal method to obtain colored titania for the photocatalytic removal of the total phenolic fraction recovered from pomace olive mill effluent (POME); reactive species formed under visible illumination cleave the aromatic rings of these phenolics, converting them into innocuous small molecules, and for simulated effluents containing 800 mg/L of total phenols, 48.17% degradation is achieved within 180 min. TiO_{2-x} fabricated solvothermally by HAN et al.[84] decomposed a 200 mg/L phenol solution under visible light at a rate 5.2-fold that of standard TiO_2. ZHOU et al.[85], meanwhile, showed that their Ag/TiO_{2-x} samples stripped a 5 mg/L 2,4-dichlorophenol solution of over 99% of its content after just 2 h of visible illumination. Silver species leverage surface-plasmon-resonance effects to accelerate photogenerated-electron migration toward conduction bands of TiO_{2-x} and enhance photocatalytic performances. Principal reactive substances for 2,4-dichlorophenol degradation are •OH and O_2^-. QIAO et al.[86] integrated wet impregnation with photoreduction to build Ag/TiO2-x nanotube heterojunctions, which accomplish total mineralization of 4-nitrophenol within a mere 70 s under light covering the visible-to-near-infrared window. The catalytic pathway is illustrated in Figure 10: •OH radicals evolved on TiO_{2-x} attack phenolic substrates and convert them into simpler intermediates (such as hydroxyphenol in the course of phenol breakdown), while the silver nanoparticles expedite these transformations by accelerating charge separation through surface plasmon resonance. Subsequent multi-step oxidation and ring-opening reactions ultimately convert organic substrates into small-molecular organics, carbon dioxide, water and other inorganic substances. These experimental findings confirm that modification approaches — whether doping or composite formation — can markedly strengthen the ability of TiO_{2-x} to photocatalytically decompose phenolic pollutants. Subsequent work would profitably target finer architectural engineering and enhanced robustness of these materials in pursuit of yet higher degradation performance.

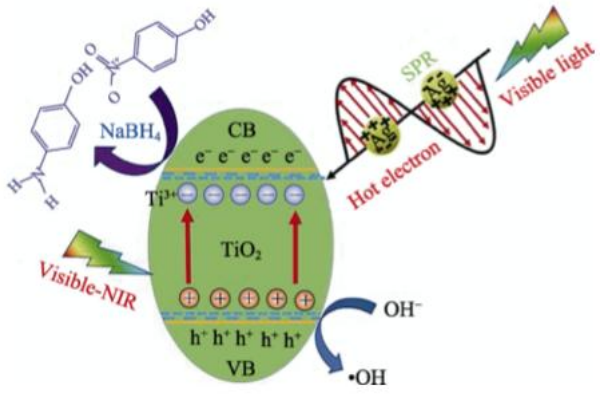

Figure 10 Schematic diagram of photocatalytic mechanism of Ag/TiO2–x nanotube heterojunction[86]

5.3 Degradation of Pharmaceutical Pollutants

Pharmaceutical residues such as antibiotics existing inside aquatic environments can inhibit or kill aquatic microorganisms and disrupt ecological equilibriums. TiO_{2-x} and its hybrid counterparts also serve as potent, eco-compatible tools for purging pharmaceutical residues from water[87]. Using TiO_{2-x} derived from ethanol-mediated reduction, BAZZANELLA et al.[88] treated ciprofloxacin solutions (10 mg/L initial concentration) and secured 95% degradation in 60 min; the transformation proceeds chiefly through photogenerated holes and •OH radicals, which strip carboxyl and acetyl groups from ciprofloxacin, curtailing its molecular weight. FENG et al.[89] followed a solvothermal step with phosphorization to coat carbon nanotubes with oxygen-vacancy/phosphorus co-doped titania (OVPTCN); this composite eliminated 87% of a 5 mg/L acetaminophen solution in 40 min, benefiting from the phosphorus-induced bandgap contraction and enhanced photon capture, with holes and •OH driving acetaminophen hydroxylation. High-temperature hydrogen reduction has likewise been exploited by WU et al.[90] to generate TiO_{2-x}. It achieves 66.2 % tetracycline degradation efficiency for initial 10 mg/L tetracycline solutions within 240 min. Degradation mechanisms rely upon redox reactions triggered by photogenerated O_2^- and h^+ toward tetracycline molecules. REN et al.[91] constructed heterojunctions assembled from hydrogen-reduced TiO_{2-x} and ultrathin gamma-Fe2O3 nanosheets for tetracycline degradation at initial mass-concentration of 10 mg/L, realizing 99.3 % degradation efficiency at 50 min. Photogenerated electrons located on conduction bands of TiO_{2-x} readily migrate toward Fe2O3 components, elevating surface-produced O_2^- concentrations and accelerating electron-hole-pair separation to boost photocatalytic performances. Quenching experiments complemented by spectroscopic evidence show that the heterojunction liberates •OH, O_2^-, and H2O2, which selectively strike the phenolic and amino moieties of tetracycline where electron density is greatest; the molecule is thereby dismantled stepwise into small intermediates that are finally oxidized to carboxylic acids, closing the degradation sequence. In another architecture, HE et al.[92] stitched reduced graphene oxide (RGO), black-TiO2 nanosheets, and two-dimensional ZIF-8 sheets (2D-ZIF-8) together with polyvinylpyrrolidone (PVP) as the linker, affording the ternary composite RGO/B-TiO2/2D-ZIF-8; under a xenon lamp, this system degraded 76% of a 25 mg/L doxycycline-hyclate solution in 120 min. Upon visible excitation, electrons (e- flow from the conduction band of 2D-ZIF-8 into that of TiO_{2-x} while holes h+ shuttle in reverse, out of the TiO_{2-x} valence band into 2D-ZIF-8. Notably, the O_2^- couple (±0.33 eV vs. NHE) lies negative of the TiO_{2-x} conduction band, so electrons accumulated on TiO_{2-x} cannot convert O2 into O_2^-; symmetrically, the 2D-ZIF-8 valence band at 0.34 eV falls far short of the H2O/•OH threshold (2.53 eV vs. NHE). Consequently, holes cannot produce •OH radicals via reaction with water molecules. Only photogenerated h+ directly participate in oxidative reactions consuming doxycycline hyclate throughout degradation workflows. Taken together, pharmaceutical-molecule degradation utilizing TiO_{2-x} and its composite systems involves oxidative degradation driven by diverse reactive-substance species. Degradation and mineralization of pharmaceutical contaminants are realized via molecular-structure hydroxylation, ring-opening and other transformation pathways.

5.4 Degradation of Other Pollutants

The utility of TiO_{2-x} and its composites extends past dye and drug removal to encompass heavy metals like Cr(VI)

as well as organic contaminants such as aniline. Sodium-borohydride reduction enabled CAO et al.[93] to produce black mesoporous TiO_{2-x} that, illuminated with visible light, cleared 95% of the Cr(Ⅵ) present in a 5 mg/L solution over 210 min. Adopting the same reductant, YAN et al.[94] crafted microporous-shelled TiO_{2-x} and achieved a 92.3% Cr(Ⅵ) removal from a 20 mg/L solution after only 60 min of visible-light exposure. Plausible mechanisms state that photogenerated electrons produced upon visible-light illumination over TiO_{2-x} react with Cr(Ⅵ) dissolved in aqueous media and reduce Cr(Ⅵ) into Cr(Ⅲ). Chromium(Ⅲ) precipitates out of aqueous solutions in the form of chromium-hydroxide $Cr(OH)_3$ precipitates and gets separated, fulfilling Cr(Ⅵ)-removal objectives. Relevant removal mechanisms are expressed in Equation (1) and Equation (2):

$$Cr_2O_7^{2-}+14H^++6(e^-CB)\rightarrow 2Cr^{3+}+7H_2O \quad (1)$$

$$Cr_2O_7^{2-}+7H_2O+6(e^-CB)\rightarrow 2Cr(OH)_3\downarrow+8OH^- \quad (2)$$

LI et al.[95] treated titanium substrates within ionic-liquid media containing lithium acetate (LiAc) and acetic acid (HAc) under mild ion-exchange circumstances and manufactured TiO_{2-x} . Under visible-light illumination, it attains 60 % aniline C6H7N degradation efficiency for initial 10 mg/L aniline solutions within 4 h. Degradation mechanisms entail reactions occurring between aniline and reactive-radical species generating intermediate products including nitrobenzene, azobenzene and so forth. Under continued photocatalytic action, these intermediates are progressively broken down into smaller species and are ultimately mineralized into innocuous products including NH_4^+, NO_3^-, and CO_2. The associated degradation reactions are expressed in Equation (3) and Equation (4):

$$TiO_{2-x}+h\nu\rightarrow TiO_2(h^+VB+e^-CB) \quad (3)$$

$$TiO_2(h^+VB)/\bullet OH+C_6H_7N\rightarrow C_6H_5NO_2/C_{12}H_{10}N_2\rightarrow NH_4^++NO_3^-+CO_2\uparrow \quad (4)$$

In summary, during photocatalytic-degradation processes for aquatic contaminants adopting TiO_{2-x} and its composite derivatives, alterations of electron-transport pathways bring about changes in dominant reactive groups participating in reactions. Hence, investigations focusing upon photocatalytic mechanisms carry great significance for governing water-pollutant-degradation behaviors and furnish theoretical foundations for high-efficiency elimination of diverse pollutant varieties.

6 Conclusions and Outlook

Synthetic-condition selections for titania directly dictate color, architectures and performances of as-prepared TiO_{2-x} . Its favorable optical, chemical and electronic performances originate from diverse intrinsic defects including surface disorder, oxygen vacancies and Ti^{3+}. Relevant research demonstrates promising application potential for TiO_{2-x} , which drives continuous optimization and upgrading for its synthetic workflows. Synthetic approaches have progressed away from hazardous high-temperature reduction with hydrogen gas toward gentler alternatives, encompassing reductions mediated by milder reductants, electrochemical routes, oxidation of low-valent titanium compounds, sonochemical processing, and laser-based modification. Even so, although TiO_{2-x} already performs impressively, its single-component form still falls short of practical expectations with respect to electron-transport channels and visible-light responsiveness. Remedies including metal deposition, non-metal doping, heterojunction engineering, and integration with adsorbent supports curb the recombination of photogenerated carriers while strengthening light harvesting, thereby securing superior real-world performance in water-pollution remediation.

Even though TiO_{2-x} and its composite materials achieve satisfactory outcomes for aquatic-pollution remediation, multiple challenges persist for its future development.

(1) Producing TiO_{2-x} and its composite counterparts typically entails elaborate, multi-stage procedures — from feedstock selection and pre-treatment through performance optimization to product separation — all of which

add manufacturing complexity and demanding technical thresholds. A pressing need therefore exists for TiO_{2-x}-based composites that combine structural robustness with simplified processing, alongside a clearer mechanistic picture of how their photocatalytic active centers cooperate.

(2) Creating oxygen vacancies at the surface contracts the bandgap and benefits photocatalytic activity; however, the vacancy concentration achieved in practice is seldom controllable, and evidence indicates that an overabundance of vacancies in fact hastens carrier recombination, eroding catalytic performance. There is thus a clear need for preparation strategies that regulate vacancy levels with precision while remaining green, inexpensive, energy-efficient, and procedurally straightforward — promising directions include innovative surface-modification techniques and machine-learning-guided tuning of oxygen-vacancy and Ti^{3+} populations.

(3) Given the impressive capabilities demonstrated by TiO_{2-x} and its hybrid derivatives, subsequent studies would do well to broaden their scope toward trace-level and emerging pollutants — microplastics and endocrine disruptors being prime examples, given their pronounced mobility and toxicity.

(4) When deployed in water-purification and other application scenarios, TiO_{2-x} and its composites face difficulties in complete recovery from reaction systems, which restricts their practical applications. Fabricating magnetic or non-powdery TiO_{2-x} is expected to promote its popularization in practical scenarios.

To sum up, TiO_{2-x} and its composite materials deliver favorable photocatalytic degradation performances, especially for photocatalytic removal of water-borne pollutants. Further development of stable and facile preparation-optimization strategies is required in future work, so as to improve its recoverability and industrial potential and realize broader environmental-protection-oriented applications.

References

[1] INNOCENZI P, MALFATTI L. Mesoporous ordered titania films: An advanced platform for photocatalysis[J]. Journal of Photochemistry and Photobiology C: Photochemistry Reviews, 2024, 58: 100646.

[2] MULAY M R, PATWARDHAN S V, MARSINOVICH N. Review of bio-inspired green synthesis of titanium dioxide for photocatalytic applications[J]. Catalysts, 2024, 14(11): 742.

[3] ARUN J, NACHIAPPAN S, RANGARAJAN G, et al. Synthesis and application of titanium dioxide photocatalysis for energy, decontamination and viral disinfection: A review[J]. Environmental Chemistry Letters, 2023, 21(1): 339-362.

[4] GONG Y Y, CAO Y L, GAO M C, et al. Properties of oxygen-rich vacancy nano-\(TiO_2\) photocatalytic preparation of \(H_2O_2\)[J]. Fine Chemicals, 2024, 41(12): 2737-2743, 2784.

[5] CHO M S, YOUNIS S A, LEE C S, et al. The superior mineralization potential of a graphitic carbon nitride/titanium dioxide composite and its application in the construction of a portable photocatalytic air purification system against gaseous formaldehyde[J]. Journal of Materials Chemistry A, 2024, 12(46): 32239-32258.

[6] NAKAMOTO R, OKAZAKI H, WAKITA T, et al. Effects of thermal energy on the formation of lattice strain in VO2 thin films grown onTiO2 (001)[J]. Langmuir, 2024, 40(46): 24447-24454.

[7] BOYD C, MCBRIDE S, PAOLINO M, et al. Assigning surface hole polaron configurations of titanium oxide materials to excited-state optical absorptions[J]. Journal of the American Chemical Society, 2025, 147(13): 10981-10991.

[8] CHEN X B, LU L, YU P Y, et al. Increasing solar absorption for photocatalysis with black hydrogenated titanium dioxide nanocrystals[J]. Science, 2011, 331(6018): 746-750.

[9] LI N, ZHANG W, LI G X, et al. Research progress onTiO2 photocatalysts[J]. Fine Chemicals, 2021, 38(11): 2181-2188, 2258.

[10] FUENTES K M, VENUTI D, BETANCOURT P. Black titania with increased defective sites for phenol photodegradation under visible light[J]. Reaction Kinetics, Mechanisms and Catalysis, 2020, 131(1): 423-435.

[11] ANDRONIC L, LELIS M, ENESCA A, et al. Photocatalytic activity of defective black-titanium oxide photocatalysts towards pesticide degradation under UV/Vis irradiation[J]. Surfaces and Interfaces, 2022, 32: 102123.

[12] KHANAM R, TAPARIA D, MOMDAL B, et al. Black titania: Effect of hydrogenation on structural and thermal stability of nanotitania[J]. Applied Physics A, 2016, 122(2): 92.
[13] THAKUR N, THAKUR N, KUMAR A, et al. A critical review on the recent trends of photocatalytic, antibacterial, antioxidant and nanohybrid applications of anatase and rutileTiO2 nanoparticles[J]. Science of the Total Environment, 2024, 914: 169815.
[14] HAIDER S, NAWAZ R, ANJUM M, et al. Property-performance relationship of core-shell structured blackTiO2 photocatalyst for environmental remediation[J]. Frontiers of Environmental Science & Engineering, 2023, 17(9): 111.
[15] LIN L X, HUANG J T, LI X F, et al. Effective surface disorder engineering of metal oxide nanocrystals for improved photocatalysis[J]. Applied Catalysis B: Environmental, 2017, 203: 615-624.
[16] SORIA J, SANZ J, TORRALVO M J, et al. The effect of the surface disordered layer on the photoreactivity of titania nanoparticles[J]. Applied Catalysis B: Environmental, 2017, 210: 306-319.
[17] LI Z, WANG E G, ZHANG Y Z, et al. Antibacterial ability of black titania in dark: Via oxygen vacancies mediated electron transfer[J]. Nano Today, 2023, 50: 101826.
[18] JIANG W B, LOH H Y, LOW B Q L, et al. Role of oxygen vacancy in metal oxides for photocatalytic \(CO_2\) reduction[J]. Applied Catalysis B: Environmental, 2023, 321: 122079.
[19] WANG G J, ZHENG J, BI H, et al. Ti^{3+} self-doping in bulk of rutileTiO2 for enhanced photocatalysis[J]. Scripta Materialia, 2019, 162: 28-32.
[20] DESKINS N A, DU J, RAO P. The structural and electronic properties of reduced amorphous titania[J]. Physical Chemistry Chemical Physics, 2017, 19(28): 18671-18684.
[21] WANG D, ZHENG S Y, YAO J, et al. A novel 3DOM Ti^{3+} self-dopedTiO2 for photocatalytic removal of NO[J]. Chemical Physics Letters, 2019, 716: 215-220.
[22] LIU X G, BI Y P. Synergistic effect of Ti^{3+} doping and facet regulation over Ti^{3+}-dopedTiO2 nanosheets with enhanced photoreactivity[J]. Catalysis Science & Technology, 2018, 8(15): 3876-3882.
[23] ABDULLAH S A, SAHDAN M Z, NAFARIZAL N, et al. Influence of substrate annealing on inducing Ti^{3+} and oxygen vacancy inTiO2 thin films deposited via RF magnetron sputtering[J]. Applied Surface Science, 2018, 462: 575-582.
[24] IVANOVSKAYA M, CHERNYakova K, OYODOK E, et al. Synthesis and structural features of blackTiO2 nanotubes after annealing in hydrogen[J]. Materials Chemistry and Physics, 2023, 297: 127416.
[25] GAO X T. Study on photocatalytic properties based on TiO_{2-x} and its composites[D]. Harbin: Harbin Normal University, 2022.
[26] HE M, JI J, LIU B Y, et al. ReducedTiO2 with tunable oxygen vacancies for catalytic oxidation of formaldehyde at room temperature[J]. Applied Surface Science, 2019, 473: 934-942.
[27] CHEN J, DING Z Y, WANG C, et al. Black anatase titania with ultrafast sodium-storage performances stimulated by oxygen vacancies[J]. ACS Applied Materials & Interfaces, 2016, 8(14): 9142-9151.
[28] SHI D X, ZHANG H H, GAO X, et al. Research progress on the preparation and catalytic application of core-shell nanocomposites[J]. Fine Chemicals, 2023, 40(1): 33-43.
[29] HU W Y, ZHOU W, ZHANG K F, et al. Facile strategy for controllable synthesis of stable mesoporous blackTiO2 hollow spheres with efficient solar-driven photocatalytic hydrogen evolution[J]. Journal of Materials Chemistry A, 2016, 4(19): 7495-7502.
[30] ZHANG K, PARK J H. Surface localization of defects in blackTiO2: Enhancing photoactivity or reactivity[J]. The Journal of Physical Chemistry Letters, 2017, 8(1): 199-207.
[31] ZHANG S S, ZHANG S Q, PENG B Y, et al. High performance hydrogenatedTiO2 nanorod arrays as a photoelectrochemical sensor for organic compounds under visible light[J]. Electrochemistry Communications, 2014, 40: 24-27.
[32] WANG Z, YANG C Y, LIN T, et al. H-doped black titania with very high solar absorption and excellent photocatalysis enhanced by localized surface plasmon resonance[J]. Advanced Functional Materials, 2013, 23(43): 5444-5450.
[33] PYLNEV M, CHANG W H, WONG M S. Shell of black titania prepared by sputteringTiO2 target in H2+Ar plasma[J]. Applied Surface Science, 2018, 462: 285-290.
[34] ARIYANTI D, MILLS L, DONG J, et al. \(NaBH_4\) modifiedTiO2: Defect site enhancement related to its photocatalytic activity[J]. Materials Chemistry and Physics, 2017, 199: 571-576.
[35] CHEN S H, XIAO Y, WANG Y H, et al. A facile approach to prepare blackTiO2 with oxygen vacancy for enhancing photocatalytic activity[J]. Nanomaterials, 2018, 8(4): 245.
[36] ZHENG P, TANG J L, ZHOU Z P, et al. Ultrafast synthesis of defective blackTiO2 via one-step \(NaN_3\)

deflagration for high-efficiency solar water evaporation[J]. Surfaces and Interfaces, 2020, 22: 100901.
[37] WANG Z, YANG C Y, LIN T Q, et al. Visible-light photocatalytic, solar thermal and photoelectrochemical properties of aluminium-reduced black titania[J]. Energy & Environmental Science, 2013, 6(10): 3007-3014.
[38] LIN L X, HUANG J T, LI X F, et al. Effective surface disorder engineering of metal oxide nanocrystals for improved photocatalysis[J]. Applied Catalysis B: Environmental, 2017, 203: 615-624.
[39] AZAB N A, EL-SHARKAWY A A M, OMRAN Z A, et al. \(C_3N_4\) interlayer formation while synthesizing black titania and their dye sensitized solar cell and conductivity performances[J]. Solar Energy Materials and Solar Cells, 2021, 232: 111347.
[40] QI W T, WANG N, CHEN X Y, et al. Plasmon-assisted partially reducedTiO2 nanotube arrays for photoelectrochemical water splitting[J]. Materials Research Express, 2020, 6(12): 1250h9.
[41] LI Z B, BIAN H D, XIAO X F, et al. Defective blackTiO2 nanotube arrays for enhanced photocatalytic and photoelectrochemical applications[J]. ACS Applied Nano Materials, 2019, 2(11): 7372-7378.
[42] LIU X, XU H, GRABSTANOWICZ L R, et al. \(Ti^{3+}\) self-doped TiO_{2-x} anatase nanoparticles via oxidation of \(TiH_2\) in \(H_2O_2\)[J]. Catalysis Today, 2014, 225: 80-89.
[43] REDDY Y A K, KANG I K, SHIN Y B, et al. Oxygen atmosphere annealing effect on the thermal stability of TiO_{2-x} based films for shutter-less infrared image sensors[J]. Key Engineering Materials, 2018, 775: 272-277.
[44] SU Y, ZHANG W, CHEN S M, et al. Engineering black titanium dioxide by femtosecond laser filament[J]. Applied Surface Science, 2020, 520: 146298.
[45] JEDSUKONTORN T, UENO T, SAITO N, et al. Facile preparation of defective blackTiO2 through the solution plasma process: Effect of parametric changes for plasma discharge on its structural and optical properties[J]. Journal of Alloys and Compounds, 2017, 726: 567-577.
[46] RAES A, NINAKANTI R, Van den B L, et al. Black titania by sonochemistry: A critical evaluation of existing methods[J]. Ultrasonics Sonochemistry, 2023, 100: 106601.
[47] ZHANG L N, LIU T L, LIU T F, et al. Improving photocatalytic performance of defective titania for carbon dioxide photoreduction by Cu cocatalyst with SCN-ion modification[J]. Chemical Engineering Journal, 2023, 463: 142358.
[48] BI Q Y, SONG E, CHEN J C, et al. Nano gold coupled black titania composites with enhanced surface plasma properties for efficient photocatalytic alkyne reduction[J]. Applied Catalysis B: Environmental, 2022, 309: 121222.
[49] CONG T Z, ZHANG Y F, HUANG H, et al. Ag nanoparticles synthesized on black-titanium dioxide by photocatalytic method as reusable substrates of surface-enhanced Raman spectroscopy[J]. Chemosensors, 2022, 10(11): 441.
[50] YUAN C F, SHEN Y L, ZHU C Y, et al. Ru single-atom decorated blackTiO2 nanosheets for efficient solar-driven hydrogen production[J]. ACS Sustainable Chemistry & Engineering, 2022, 10(31): 10311-10317.
[51] YUAN X T, WANG X, LIU X Y, et al. \(Ti^{3+}\)-promoted high oxygen-reduction activity of Pd nanodots supported by black titania nanobelts[J]. ACS Applied Materials & Interfaces, 2016, 8(41): 27654-27660.
[52] YANG C Y, WANG Z, LIN T Q, et al. Core-shell nanostructured "black" rutile titania as excellent catalyst for hydrogen production enhanced by sulfur doping[J]. Journal of the American Chemical Society, 2013, 135(47): 17831-17838.
[53] RAHMAN S, NAWAZ R, KHAN J, et al. Synthesis and characterization of carbon and carbon-nitrogen doped blackTiO2 nanomaterials and their application in sonophotocatalytic remediation of treated agro-industrial wastewater[J]. Materials, 2021, 14(20): 6175.
[54] SHAFIEE A, CARRIER A J, NGANOU C, et al. Mechanistic insight into the enhanced photodegradation by black titanium dioxide nanofiber-graphene quantum dot composites[J]. Applied Surface Science, 2023, 636: 157836.
[55] DONG X F, LI H Q, GUO Y, et al. Construction of hierarchical blackTiO2/carbon fiber: Enhanced photocatalytic activity based on schottky heterojunctions[J]. ACS Applied Bio Materials, 2024, 7(8): 5397-5410.
[56] LIANG Y, HUANG G H, XIN X Y, et al. Black titanium dioxide nanomaterials for photocatalytic removal of pollutants: A review[J]. Journal of Materials Science & Technology, 2022, 112: 239-262.
[57] CUI H, CAO J Y, ZHAO Y, et al. Construction of IO-B-\(TiO_2\)/\(In_2O_3\) S-scheme heterojunction with photothermal effects and its highly efficient photocatalytic reduction of \(CO_2\) under full-spectrum light[J]. Chemical Engineering Journal, 2024, 479: 147618.
[58] LI Y F, FENG Y C, BAI H, et al. Enhanced visible-light photocatalytic performance of blackTiO2/\(SnO_2\) nanoparticles[J]. Journal of Alloys and Compounds, 2023, 960: 170672.
[59] LI Z Z, LI H Z, WANG S J, et al. Mesoporous blackTiO2/\(MoS_2\)/\(Cu_2S\) hierarchical tandem

heterojunctions toward optimized photothermal-photocatalytic fuel production[J]. Chemical Engineering Journal, 2022, 427: 131830.

[60] TAN B Y, YE X Z, LI Y J, et al. Defective anatase TiO_{2-x} mesocrystal growth in situ on \(g-C_3N_4\) nanosheets: Construction of 3D/2D Z-scheme heterostructures for highly efficient visible-light photocatalysis[J]. Chemistry-A European Journal, 2018, 24(50): 13311-13321.

[61] LI J, JIANG Z X, LI J F, et al. Synthesis of black titanium dioxide/activated carbon composites for enhanced visible-light photocatalytic properties[J]. Journal of Materials Science: Materials in Electronics, 2024, 35(16): 1050.

[62] ZAKARIA H, LI Y, FATHY M M, et al. A novel TiO_{2-x} /TiN@ACB composite-for synchronous photocatalytic Cr(Ⅵ) reduction and water photothermal evaporation under visible/infrared light illumination[J]. Chemosphere, 2023, 311: 137137.

[63] HU P W, ZHANG Y, CHENG G L. Natural kaolinite modified black titanium dioxide for efficient visible light assisted photocatalysis[J]. Molecular Catalysis, 2023, 547: 113312.

[64] KHAN S, NOOR T, IQBAL N, et al. Photocatalytic dye degradation from textile wastewater: A review[J]. ACS Omega, 2024, 9(20): 21751-21767.

[65] LIN J Y, YE W Y, XIE M, et al. Environmental impacts and remediation of dye-containing wastewater[J]. Nature Reviews Earth & Environment, 2023, 4(11): 785-803.

[66] BUZZETTI L, CRISENZA G E M, MELCHIORRE P. Mechanistic studies in photocatalysis[J]. Angewandte Chemie International Edition, 2019, 58(12): 3730-3747.

[67] ZHAI M J, LIU Y, HUANG J, et al. Efficient suspension plasma spray fabrication of black titanium dioxide coatings with visible light absorption performances[J]. Ceramics International, 2019, 45(1): 930-935.

[68] CHEN S H, WANG Y H, LI J, et al. Synthesis of blackTiO2 with efficient visible-light photocatalytic activity by ultraviolet light irradiation and low temperature annealing[J]. Materials Research Bulletin, 2018, 98: 280-287.

[69] SAENSOOK S, SIRISUK A. A factorial experimental design approach to obtain defect-rich blackTiO2 for photocatalytic dye degradation[J]. Journal of Water Process Engineering, 2022, 45: 102495.

[70] YUAN X J, SUN M X, YAO Y, et al. N/Ti3+-codoped triphasicTiO2/g-C3N4 heterojunctions as visible-light photocatalysts for the degradation of organic contaminants[J]. New Journal of Chemistry, 2019, 43(6): 2665-2675.

[71] CHEN P. A novel synthesis of Ti3+ self-doped Ag2O/TiO2 (p-n) nanoheterojunctions for enhanced visible photocatalytic activity[J]. Materials Letters, 2016, 163: 130-133.

[72] WANG S C, CAI J S, MAO J J, et al. Defective black Ti3+ self-dopedTiO2 and reduced graphene oxide composite nanoparticles for boosting visible-light driven photocatalytic and photoelectrochemical activity[J]. Applied Surface Science, 2019, 467: 45-55.

[73] LI J, JIANG Z X, LI J F, et al. Synthesis of black titanium dioxide/activated carbon composites for enhanced visible-light photocatalytic properties[J]. Journal of Materials Science: Materials in Electronics, 2024, 35(16): 1050.

[74] JIANG X D, ZHANG Y P, JIANG J, et al. Characterization of oxygen vacancy associates within hydrogenatedTiO2: A positron annihilation study[J]. The Journal of Physical Chemistry C, 2012, 116(42): 22619-22624.

[75] PRADENAS M, YÁÑEZ J, RANGANATHAN S, et al. Multivariate approach to hydrogenatedTiO2 photocatalytic activity under visible light[J]. Water Environment Research, 2019, 91(2): 157-164.

[76] AN H R, PARK S Y, KIM H, et al. Advanced nanoporousTiO2 photocatalysts by hydrogen plasma for efficient solar-light photocatalytic application[J]. Scientific Reports, 2016, 6(1): 29683.

[77] WANG X T, LI Y M, LIU X, et al. Preparation of Ti3+ self-dopedTiO2 nanoparticles and their visible light photocatalytic activity[J]. Chinese Journal of Catalysis, 2015, 36(3): 389-399.

[78] HAN K, ZHANG X, WANG H F, et al. A facile microwaving method to turn titanium oxide into highly active Ti^{3+} self-doped structure[J]. Journal of Nanoscience and Nanotechnology, 2016, 16(9): 9826-9831.

[79] LI G L, LI J, LI G, et al. N and Ti3+ co-doped 3D anataseTiO2 superstructures composed of ultrathin nanosheets with enhanced visible light photocatalytic activity[J]. Journal of Materials Chemistry A, 2015, 3(44): 22073-22080.

[80] ZHANG H, XING Z P, ZHANG Y, et al. Ni2+) and Ti3+ co-doped porous black anataseTiO2 with unprecedented-high visible-light-driven photocatalytic degradation performance[J]. RSC Advances, 2015, 5(129): 107150-107157.

[81] DU J M, WANG H M, CHEN H J, et al. Synthesis and enhanced photocatalytic activity of black porous Zr-dopedTiO2 monoliths[J]. Nano, 2016, 11(6): 1650068.
[82] YADAV G, AHMARUZZAMAN M. New generation advanced nanomaterials for photocatalytic abatement of phenolic compounds[J]. Chemosphere, 2022, 304: 135297.
[83] NAWAZ R, KAIT C F, CHIA H Y, et al. Glycerol-mediated facile synthesis of colored titania nanoparticles for visible light photodegradation of phenolic compounds[J]. Nanomaterials, 2019, 9(11): 1586.
[84] HAN L J, SU B T, LIU G, et al. Synthesis of oxygen vacancy-rich blackTiO2 nanoparticles and the visible light photocatalytic performance[J]. Molecular Catalysis, 2018, 456: 96-101.
[85] ZHOU G, MENG H Y, CAO Y, et al. Surface plasmon resonance-enhanced solar-driven photocatalytic performance from Ag nanoparticles-decorated \(Ti^{3+}\) self-doped porous blackTiO2 pillars[J]. Journal of Industrial and Engineering Chemistry, 2018, 64: 188-193.
[86] QIAO P Z, SUN B J, LI H Z, et al. Surface plasmon resonance-enhanced visible-NIR-driven photocatalytic and photothermal catalytic performance by Ag/mesoporous blackTiO2 nanotube heterojunctions[J]. Chemistry-An Asian Journal, 2019, 14(1): 177-186.
[87] RUZIWA D T, OLUWALANA A E, MUPA M, et al. Pharmaceuticals in wastewater and their photocatalytic degradation using nano-enabled photocatalysts[J]. Journal of Water Process Engineering, 2023, 54: 103880.
[88] BAZZANELLA N, BAJPAI O P, FENDRICH M, et al. Ciprofloxacin degradation with a defective TiO_{2-x} nanomaterial under sunlight[J]. MRS Communications, 2023, 13(6): 1252-1259.
[89] FENG X Y, WANG P F, HOU J, et al. Oxygen vacancies and phosphorus codoped black titania coated carbon nanotube composite photocatalyst with efficient photocatalytic performance for the degradation of acetaminophen under visible light irradiation[J]. Chemical Engineering Journal, 2018, 352: 947-956.
[90] WU S Q, LI X Y, TIAN Y Q, et al. Excellent photocatalytic degradation of tetracycline over black anatase-TiO2 under visible light[J]. Chemical Engineering Journal, 2021, 406: 126747.
[91] REN L P, ZHOU W, SUN B J, et al. Defects-engineering of magnetic gamma-Fe2O3 ultrathin nanosheets/mesoporous blackTiO2 hollow sphere heterojunctions for efficient charge separation and the solar-driven photocatalytic mechanism of tetracycline degradation[J]. Applied Catalysis B: Environmental, 2019, 240: 319-328.
[92] HE J H, YE J, ZHANG Y, et al. Synergistic RGO/blackTiO2/2D-ZIF-8 ternary heterogeneous composite with highly efficient photocatalytic activity[J]. ChemistrySelect, 2020, 5(12): 3746-3755.
[93] CAO Y, XING Z P, HU M Q, et al. Mesoporous black N-TiO_{2-x} hollow spheres as efficient visible-light-driven photocatalysts[J]. Journal of Catalysis, 2017, 356: 246-254.
[94] YAN Z Y, HUANG W X, JIANG X R, et al. Hollow structured blackTiO2 with thickness-controllable microporous shells for enhanced visible-light-driven photocatalysis[J]. Microporous and Mesoporous Materials, 2021, 323: 111228.
[95] LI G S, LIAN Z C, LI X, et al. Ionothermal synthesis of black Ti^{3+}-doped single-crystalTiO2 as an active photocatalyst for pollutant degradation and H2 generation[J]. Journal of Materials Chemistry A, 2015, 3(7): 3748-3756.